Cell motility in confluent tissues induced by substrate disorder

Diogo E. P. Pinto ⬤, Margarida M. Telo da Gama ⬤, and Nuno A. M. Araújo ⬤

Centro de Física Teórica e Computacional, Faculdade de Ciências, Universidade de Lisboa, 1749-016 Lisboa, Portugal
and Departamento de Física, Faculdade de Ciências, Universidade de Lisboa, 1749-016 Lisboa, Portugal

In vivo and *in vitro* cells rely on the support of an underlying biocompatible substrate, such as the extracellular matrix or a culture substrate, to spread and proliferate. The mechanical and chemical properties of such structures play a central role in the dynamical and statistical properties of the tissue. At the cell scale, these substrates are highly disordered. Here, we investigate how spatial heterogeneities of the cell-substrate interaction influence the motility of the cells in a model confluent tissue. We use the self-propelled Voronoi model and describe the disorder as a spatially dependent preferred geometry of the individual cells. We found that when the characteristic length scale of the preferred geometry is smaller than the cell size, the tissue is less rigid than its homogeneous counterpart, with a consequent increase in cell motility. This result is in sharp contrast to what has been reported for tissues with heterogeneity in the mechanical properties of the individual cells, where the disorder favors rigidity. Using the fraction of rigid cells, we observe a collapse of the motility data for different model parameters and provide evidence that the rigidity transition in the model tissue is accompanied by the emergence of a spanning cluster of rigid cells.

I. INTRODUCTION

The idea of growing artificial cell tissues and organs has been around for several decades [1,2]. This has spurred a truly multidisciplinary effort to understand the mechanisms responsible for the development of cell tissues and to search for novel strategies to tune the shape and mechanical properties of the tissue. Among those strategies is the use of biocompatible substrates [1,3,4]. An extensive body of research shows that the cell morphology and dynamics are sensitive to the physical and chemical properties of their underlying structure, be it the extracellular matrix or a culture substrate [5–13]. For example, it has been shown that the substrate stiffness can significantly affect the geometry of cultured cells, including their spreading area [13,14], volume [15], and shape elongation [16]. The mechanical properties of cells have been shown to change when they adhere to substrates due to the influence of cell-matrix adhesion complexes; for example, cells adhered to rigid substrates develop stresses at the level of the actin network which lead to polarization [17]. Recent studies have also shown that the nanotopography of the substrate can significantly change the cell shape and motility [18–21]. Thus, irrespective of the biological effects, the physical interaction between the cells and their supporting structure plays a critical role in the mechanical properties of the tissue. This poses a

great challenge due to the typical level of disorder involved [22–24].

Both *in vivo* and *in vitro*, the epithelial layer of cells is supported by a complex polymeric structure, the extracellular matrix (ECM), which constrains the collective behavior of the tissue [5,25–28]. For example, it has been observed that cancerous cells alter the ECM in order to promote invasion through healthy tissue [29,30]. The tumor microenvironment supports diverse mechanical and biochemical interactions during cancer progression, which plays a significant role in the degree of tumor malignancy and metastatic potential [31,32]. Tumors act as local sources of ECM remodeling, resulting in heterogeneous spatial profiles of the ECM network [33]. These profiles can then influence the migration of surrounding cells [34]. By generating cell-scaled tracks along migratory paths, cells will not need to squeeze through or clear constrictive mechanical barriers [34]. Thus, although the ECM is often quantified by bulk metrics, it has a high degree of heterogeneity, which in turn influences the tissue itself, in a way that is largely unclear.

Despite the broad range of physicochemical processes, which in many cases are system dependent [2], there are convincing arguments that simple, mechanistic models can provide valuable insight into the dynamics of living systems [35–38]. Several models have been proposed to understand their collective behavior, from single-particle descriptions to density field models [35,36,38–43]. The self-propelled Voronoi model (SPV) has been one of the models of choice to study confluent tissues [44,45]. The degrees of freedom are the positions of the center of each cell and the cell shape is obtained by Voronoi tessellation [46]. The dynamics is governed by an energy functional that is quadratic in the area and perimeter of each (Voronoi) cell, thus making the interactions
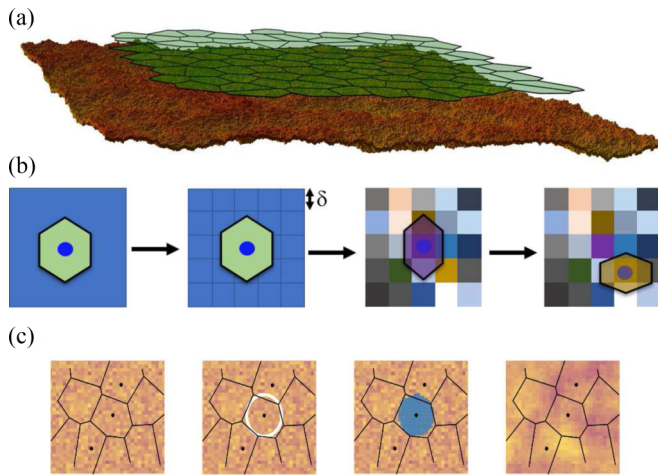
FIG. 1. (a) Illustration of the model. We consider the two-dimensional (2D) projection of the tissue (top, in green), described using the self-propelled Voronoi model, on a 2D heterogeneous substrate (bottom) where the value of the target shape index of the cells depends on the position. The color of the substrate is related to the value of the shape index in the square tiles, $p_{0,j}$, with red corresponding to higher values and yellow to lower ones. The height profile in the substrate is only meant to illustrate this heterogeneity. (b) Schematic representation of the substrate implementation. We start by dividing the simulation box into squares of length δ and attribute to each square a random shape index drawn from a Gaussian distribution with mean $\bar{p}_0$ and standard deviation σ. Depending on the position of the center of the cell its shape index will change. For example, as is seen in the schematic, when it is in a purple square the cell has a purple shape index but when it changes to a yellow square the shape index changes accordingly. (c) Schematic representation of the averaging process used on the random substrate. The averaging is performed to account for the fact that a cell can sense a given space around its center. Accordingly, we consider for each cell a circular region around its center, with radius $\xi/2$ (averaging radius in white) and calculate the average shape index of all the tiles within that region. The blue shape corresponds to the square tiles used for the averaging. Here we have used approximately 80 blue square tiles, where each tile has a length two orders of magnitudes smaller than the typical length of a cell. The color of the substrate on the last panel represents the averaged substrate.

truly many body. The mechanical properties of the tissue are either solid or fluid like, depending on the strength of activity and shape parameter, p_0, of the individual cells [44]. The solid-like regime is characterized by a finite shear modulus, while in the fluid-like regime the shear modulus drops significantly [44,47]. These results agree both quantitatively and qualitatively with experiments on monolayer tissues [48,49].

Here, we investigate how heterogeneities on the substrate affect the mechanical properties of confluent tissues [see Fig. 1(a)]. We describe the confluent tissue using the self-propelled Voronoi model with a position-dependent shape parameter to account for spatial heterogeneities in the cell-substrate interaction. Previous works have established that cell shapes and the cell-cell interaction change as a function of substrate properties [7,14,16,17] and in turn the cell shape governs the rate of cell diffusion in the tissue [48]. Thus, we consider that for a given cell-substrate interaction,

the subcellular changes observed translate into different cell-cell interactions or cell shapes, which can be simplified into a position-dependent shape parameter. Heterogeneity in the mechanical properties of the individual cells is known to substantially affect cell motility [50,51]. For example, numerical simulations of the vertex model suggest that a heterogeneous distribution of the mechanical properties of individual cells favors rigidity and thus hinders cell motility [52]. This particular type of cell disorder leads to larger tensions between adhered cells, which in turn gives rise to a percolating cluster of rigid cells responsible for the increase in the tissue rigidity. This result sheds light on the dynamics of cancer propagation, for cancer cells are usually softer than healthy ones [53–55]. Here, we show that the opposite behavior is observed when the disorder is on the substrate (position dependent). For values of the characteristic length scale of the disorder lower than the typical cell size, the tissue is less rigid and cell motility is enhanced.

The paper is organized as follows. In Sec. II, we introduce the model. In Sec. III, we give an overview of the results. We consider the average diffusion coefficient of the cells to quantify the motility. In Sec. IV, we discuss the results obtained with a random substrate and discuss the collapse of the numerical data for different model parameters. In Sec. V, we focus on an averaged substrate and compare the results for three different disordered systems: cell, random, and averaged substrates. In Sec. VI, we draw some conclusions and discuss practical implications.

II. MODEL

We model the confluent tissue as a monolayer of N cells using the self-propelled Voronoi model [44]. Each cell i is represented by its center $\mathbf{r}_i$ and its shape is given by an instantaneous Voronoi tessellation of the space. The stochastic trajectory of each cell is obtained by solving a set of equations of motion in the overdamped regime,

$$\frac{d\mathbf{r}_i}{dt} = \mu \mathbf{F}_i + v_0 \hat{\mathbf{n}}_i, \tag{1}$$

where $\mathbf{F}_i$ is the net force acting on cell i, μ is the mobility of the cell, v_0 is the self-propulsion speed, and $\hat{\mathbf{n}}_i = (\cos\theta_i, \sin\theta_i)$ is a polarity vector which sets the direction of self-propulsion. For simplicity, we consider that θ_i is modeled by a stochastic process given by

$$\dot{\theta}_i = \eta_i(t), \quad \langle \eta_i(t)\eta_j(t')\rangle = 2D_r\delta(t-t')\delta_{ij}, \tag{2}$$

where $\eta_i(t)$ is an uncorrelated random process of zero mean and variance set by a rotational diffusion coefficient D_r.

The force $\mathbf{F}_i$ describes the many-body cell-cell interaction and is given by $\mathbf{F}_i = -\nabla E_i$, where E_i is the energy functional for cell i [35,36],

$$E_i = K_A[A_i - A_0]^2 + K_P[P_i - P_{0,i}]^2, \tag{3}$$

where A_i and P_i are the area and perimeter of cell i, respectively, and A_0 and $P_{0,i}$ are their target values. In this 2D representation of a confluent tissue, changes in the thickness of the cell are considered through the first term in the energy functional, Eq. (3). This term describes the resistance of the cell monolayer to height fluctuations due to cell adhesion [56].

The second term, quadratic in the perimeter, represents the active contractility of the actin-myosin cortex [36] and the interfacial tension due to the competition between cortical tension and cell-cell adhesion [57]. K_A and K_P are the area and perimeter moduli. By rescaling the energy in units of $K_A A_0^2$, we obtain four nondimensional quantities: two for the area and perimeter of the cell ($a_i = A_i/A_0$ and $p_i = P_i/\sqrt{A_0}$), a shape parameter $p_{0,i} = P_{0,i}/\sqrt{A_0}$, and the energy ratio $r = K_A A_0/K_p$ (see the Supplemental Material for details of the units system [58]). Without loss of generality, in what follows, lengths are in units of $\sqrt{A_0}$ and time is in units of $1/(\mu K_A A_0)$.

Cells diffuse with a diffusion coefficient D that depends on four model parameters: the speed of self-propulsion v_0, the rotational diffusion D_r, the shape index $p_{0,i}$ of each cell i, and the energy ratio r. In the homogeneous case ($p_{0,i} \equiv p_0$ for all cells), for fixed values of v_0 and D_r, the model exhibits a rigidity transition at a value of the shape index $p_0 = p_c$: from a fluid-like state, for $p_0 > p_c$, where the cells diffuse on the substrate ($D \neq 0$), to a solid-like state with finite shear modulus and negligible cell motility ($D \rightarrow 0$), for $p_0 < p_c$ [44,59].

We consider a square substrate of length $L = \sqrt{N}$, where the value of the target shape index ($p_{0,i}$) is spatially dependent. The substrate is divided into square tiles with length δ, in units of the cell diameter. We consider that each tile has a length two orders of magnitude smaller than the typical length of a cell. Each square tile has a value of the target parameter randomly drawn from a Gaussian distribution with mean $\bar{p}_0$ and standard deviation σ. We considered the Gaussian distribution as the simplest hypothesis to describe this heterogeneity. Throughout the dynamics, the value of the shape index, $p_{0,i}$, for each cell corresponds to the one in the underlying square tile. When a cell moves from one square tile to another, its target shape index [in Eq. (3)] changes accordingly. We expect that cells take a characteristic time to adapt to changes in the underlying substrate [60,61]. We first consider this adaptation time to be negligible small and then discuss its effect when it is comparable to the other relevant timescales.

Since cells typically spread over an area larger than that of a square tile, we consider that the cell's ability to probe its surroundings can be described, in a simplified way, as an average of the shape index over a distance on the random substrate [see Fig. 1(b)]. In order to do that, we introduce an averaged substrate, which is also square and of the same size of the original one, and thus has the same square tile length δ. The shape index on each square tile j, of the averaged substrate, is calculated by taking the average of the shape indices of the square tiles in the original substrate which have their centers at a distance less than $\xi/2$ from the center of j. Thus, for a given ξ the averaged substrate has mean $\bar{p}_0$ and standard deviation $\sigma/\sqrt{n}$, where n is the number of square tiles within the corresponding averaging circle. Some properties of the averaged substrate are further discussed in the Supplemental Material [58].

To simulate the confluent tissue, we used a hybrid CPU/GPU software package, CELLGPU [62], for the self-propelled Voronoi model. The equations of motion, Eq. (1), are integrated using the Euler method, with a time step of $\Delta t = 10^{-2}$. We impose periodic boundary conditions, $D_r = 1$, $v_0 = 0.1$, and $r = 1$. For the initial configuration, we gen-

erate N positions at random and let the system relax over 10^4 time steps. The random substrate consists of square tiles with length $\delta = 0.03125$, in units of the cell diameter. This rather small value is selected to ensure that there are no spatial correlations on the scale of the cell size and that cells are able to explore more than one substrate square tile even when they have very low motility. After the initial relaxation, the simulation is performed for another 10^6 additional time steps.

III. OVERVIEW

To characterize the fluidity of the tissue, we measure the mean squared displacement from the initial position, averaging over all the cells ($\langle \Delta r^2(t) \rangle$) and we estimate the diffusion coefficient using

$$D = \frac{\langle \Delta r^2(t) \rangle}{4t}, \quad t \gg 1. \tag{4}$$

This quantity is obtained numerically by running the simulations for 10^6 time steps and calculating the slope of a linear fit, using the least squares method, of the mean squared displacement averaged over all the cells for all time steps above 10^5. In the solid-like phase, the cells are constrained by their neighbors, they only move within an area of the order of their size, and so few cell rearrangements occur [44]. Thus, the mean squared displacement is characterized by an initial ballistic behavior ($\langle \Delta r^2 \rangle \sim t^2$) but rapidly saturates. On the other hand, in the fluid-like phase, the cells are able to break free from their cages and the tissue flows [44]. Thus, the mean squared displacement is diffusive ($\langle \Delta r^2 \rangle \sim t$) asymptotically. We have found that we can measure the diffusion coefficient reliably for time steps above 10^5, in the fluid-like phase. As the solid-like phase is approached the fitting worsens, as the diffusion coefficient decreases to zero. Nonetheless, we still use the same technique.

A recent work studied the effect of heterogeneities in the mechanical properties of individual cells using the vertex model [52]. In this study, heterogeneity is introduced at the cell level by endowing each cell with a random shape index, $p_{0,i}$, chosen from a Gaussian distribution with mean $\bar{p}_0$ and standard deviation σ. The shape index of each cell is then constant over time. It was observed that the shear modulus increases with the disorder, σ, corresponding to a more rigid tissue. In what follows, we compare the effect of the two types of disorder: substrate disorder, where the shape parameter is spatially dependent, and cell disorder, where the shape parameter is a time-independent property of the cell as discussed in Ref. [52]. For cell disorder, we have chosen the probability distribution of the shape index ($p_{0,i}$) to be Gaussian, parameterized by the same mean ($\bar{p}_0$) and standard deviation (σ). We note that both types of disorder are quenched as they do not evolve with the dynamics. Nevertheless, the substrate disorder is fixed in space, while that of the cells is carried by their motion in the fluid phase. In the rigid phase, both types of disorder are fixed in space, as cell motion practically ceases.

Figure 2 shows a diagram of the two-parameter space explored for a random substrate, where the color represents the average diffusion coefficient of the cells in the tissue using the random substrate disorder. We explored different values of the mean ($\bar{p}_0$) and standard deviation (σ) of the Gaussian
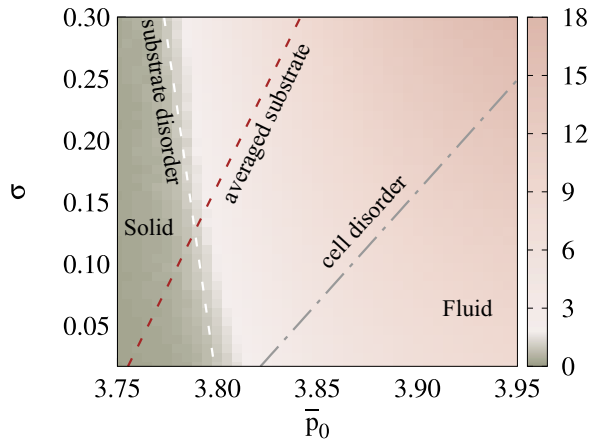
FIG. 2. Phase diagram of the tissue for substrate or cell disorder. On the vertical axis is the standard deviation of the Gaussian distribution, σ, and on the horizontal axis the mean, $\bar{p}_0$. The color gradient represents the diffusion coefficient of the tissue when using the random substrate disorder [given by Eq. (4)], in units of $D^* \approx 9.04 \times 10^{-5}$, which corresponds to the value of the diffusion coefficient at the onset of rigidity in the homogeneous system, i.e., $p_0 = 3.8$. The white (dashed) line defines the threshold where the fraction of rigid cells (cells with $p_i < 3.8$), forms a percolating cluster, $\sigma(\bar{p}_0) = -11.2\bar{p}_0 + 42.7$. Thus, it sets the onset of rigidity, in the presence of a disordered substrate. Results were obtained for $N = 1024$ and averaged over 10 samples. The gray (dot-dashed) line is obtained from Ref. [52] for a tissue with heterogeneity in the mechanical properties of individual cells described by a cell-dependent shape index $p_{0,i}$, which is also drawn from a normal distribution with the same mean and standard deviation. In this case, the onset of rigidity is given by $\sigma(\bar{p}_0) = 1.2\bar{p}_0 - 4.7$. The brown (dashed) line gives the onset of rigidity when an averaged substrate is used with correlation length of the order of the cell diameter. Here, the line is given by $\sigma(\bar{p}_0) = 3.3\bar{p}_0 - 12.5$. This figure highlights the different effects of disorder. When the disorder is at the cell level the tissue becomes more rigid, while when it is spatially dependent (i.e., on the substrate) the tissue becomes less rigid when the substrate correlation length is less than the diameter of the cells, but more rigid when it is larger. The different phases are shown in the figure, where the tissue is marked solid or fluid. The lines do not meet at $\sigma = 0$ since in Ref. [52] the vertex model was used rather than the Voronoi model used in this work.

distribution and observed that the diffusion coefficient increases for larger values of the disorder (σ), suggesting that the motility of the cells increases for substrates with larger gradients of the target shape index. We also show in the inset of Fig. 3 the increase of the diffusion coefficient with $\bar{p}_0$ and σ. This is in contrast with the cell disorder case where the rigidity of the tissue increases with increasing disorder [52].

We plot three lines that give the onset of rigidity for the different types of disorder: cell disorder and substrate disorder with and without averaging (as described in the previous section). In-depth details on how these lines are calculated are given in the following sections. We observe that the onset of rigidity in the tissue is accompanied by a percolation of rigid cells, defined as the cells with a perimeter smaller than a given shape index threshold, $p_i < \bar{p}_0^*$. When the substrate disorder is not averaged, the line is given by $\sigma(\bar{p}_0) = -11.2\bar{p}_0 + 42.7$,
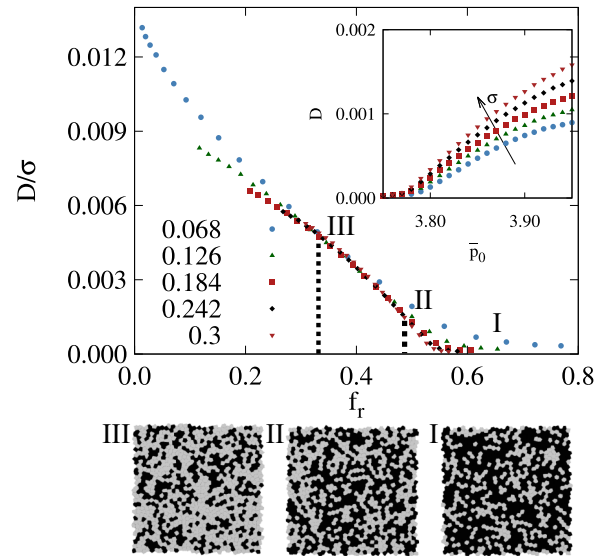

FIG. 3. Average cell diffusion coefficient as a function of the fraction of rigid cells, f_r. The diffusion coefficient is rescaled by the standard deviation σ to collapse the curves. These results were obtained for $N = 1024$, $\sigma = 0.068$–0.3 in steps of 0.058, $\bar{p}_0 = 3.75$–3.95 in steps of 0.01, and averaged over 100 samples. The scaling suggests that the fraction of rigid cells drives the rigidity transition. In the inset are the individual curves to highlight the increase of the diffusion coefficient with the disorder (σ). Below the main plot are snapshots for different fractions of rigid cells (f_r), where rigid cells in black have a shape index below a given threshold ($p_{0,i} < \bar{p}_0^*$) and fluid cells in gray have $p_{0,i} > \bar{p}_0^*$. We recall that $\bar{p}_0^* = 3.8$ is the threshold for rigid cells.

highlighting the increase in motility when the disorder (σ) increases. The cell disorder line is taken from Ref. [52], $\sigma(\bar{p}_0) = 1.2\bar{p}_0 - 4.7$, and highlights the opposite behavior. Lastly, when the substrate with averaged disorder has a correlation length of the order of the cell diameter, $\xi = 2$, the rigidity threshold is given by $\sigma(\bar{p}_0) = 3.3\bar{p}_0 - 12.5$, which also exhibits an increase of tissue rigidity with disorder (σ). Thus, while for small correlation lengths the substrate disorder promotes cell motility, for correlation lengths of the order of the cell diameter, it gives rise to tissues with increased rigidity. Furthermore, the results for the averaged substrate approach those of cell disorder as the correlation length increases, as seen in the slopes of the two lines. We hypothesize that there is a close relationship between these types of disorder. We also note that the lines do not meet at $\sigma = 0$, we hypothesize that this is because in Ref. [52] a different model, i.e., the vertex model was used. In the Supplemental Material [58] we investigate the effect of cell disorder using the Voronoi model and show that it is the same as that reported for the vertex model. Nonetheless, since the detailed mechanics of the models differ [63], the quantitative results are also different.

IV. RANDOM SUBSTRATE

First we focus on a random substrate with a square tile length smaller than the cell size (as introduced in Sec. II, $\delta = 0.03125$). To calculate the lines separating the different

regimes, we use a scaling ansatz to collapse the numerical data and estimate the transition between the solid- and fluid-like regions. In Ref. [52], a scaling ansatz is proposed for the shear modulus, which depends on the ratio between σ and the distance to a threshold $|\bar{p}_0 - \bar{p}_0^*|$, where $\bar{p}_0^*$ is the threshold value. The data were indeed observed to collapse. At $\bar{p}_0 = \bar{p}_0^*$, 50% of the cells are rigid with $p_{0,i} < \bar{p}_0^*$. This fraction decreases or increases above or below $\bar{p}_0$. This suggests that the fraction of rigid cells (cells with $p_{0,i} < \bar{p}_0^*$) plays an important role in driving the rigidity of the tissue. The fraction of rigid cells is defined as

$$f_r = \int_{-\infty}^{\bar{p}_0^*} \mathcal{F}_{\bar{p}_0,\sigma}(p_0) dp_0 = \frac{1}{2}\text{erfc}[(\bar{p}_0 - \bar{p}_0^*)/\sqrt{2}\sigma], \quad (5)$$

where σ and $\bar{p}_0$ are the standard deviation and mean of the Gaussian distribution, respectively. For substrate disorder, the cells shape index changes frequently. Thus, the probability density function should also depend on the spatial distribution of the cells and we have no control over $\mathcal{F}$ in Eq. (5). Nonetheless, for the parameters explored, we found that the cells have a distribution of the shape index, $p_{0,i}$, similar to the Gaussian used to generate the substrate disorder, with the same mean ($\bar{p}_0$) and standard deviation (σ). Thus, we use Eq. (5) to estimate the threshold of the transition, with $\bar{p}_0$ and σ the same as those used for the substrate.

Figure 3 illustrates the data collapse for the diffusion coefficient rescaled by the standard deviation as a function of the fraction of rigid cells, f_r. To collapse the different curves, we used $\bar{p}_0^* = 3.80 \pm 0.01$ in Eq. (5). We estimate this value numerically by using different threshold values ($\bar{p}_0^*$) and choosing the one for which we obtained the best data collapse. Figure 3 (bottom panels) illustrates the evolution of the rigid cluster, which corresponds to the largest cluster of rigid cells ($p_{0,i} < \bar{p}_0^*$) in black. We found that this cluster decreases as the standard deviation (σ) or the mean ($\bar{p}_0$) increase. The scaling ansatz suggests that the rigidity is driven by cells with a shape index, $p_{0,i}$, smaller than a threshold $\bar{p}_0^*$. As a result, we can estimate the onset of rigidity by measuring the threshold where the rigid cells form a system spanning cluster.

To analyze the percolation of rigid cells we measure the fraction ϕ of all rigid cells ($p_{0,i} < \bar{p}_0^*$) in the largest cluster. To estimate the percolation threshold, f_r^*, we consider the value at which the variance $\chi = \langle \phi^2 \rangle - \langle \phi \rangle^2$ is maximum. In the Supplemental Material [58], it is shown that χ has a peak around $f_r^* \approx 0.484$, signaling the onset of percolation. When comparing to the data collapse in Fig. 3, this threshold is not consistent with the point at which the diffusion coefficient starts increasing from small values ($D > 10^{-4}$). From the numerical results, the distribution of perimeters of the cells, p_i, also follows a Gaussian distribution with mean $\bar{p}_0$ and standard deviation σ. Thus, we now consider a different criteria for rigid cells. We redefine a rigid cell as one with a perimeter (p_i) below the shape index threshold, $p_i < \bar{p}_0^*$. We considered the same threshold, $\bar{p}_0^*$, since the distribution of perimeters (p_i) and shape index ($p_{0,i}$) are similar. Thus, in our case, Eq. (5) is equivalent when using the distribution for either p_i or $p_{0,i}$. We hypothesize that since p_i is related to the tension in the cells ($\tau \sim p_i - p_{0,i}$) it can also be responsible for the decreased rigidity of the tissue, as detailed in previous
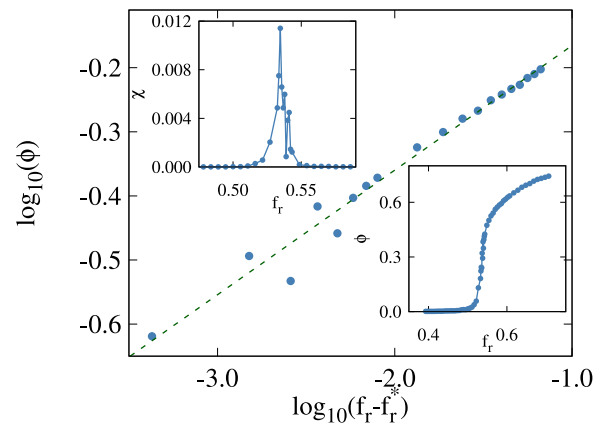

FIG. 4. Percolation at the rigidity transition. In the main plot is the fraction of rigid cells in the largest cluster, ϕ, as a function of $(f_r - f_r^*)$, where $f_r^* \approx 0.5353$ was calculated from the peak in the variance (top left inset). In the bottom right inset is ϕ as a function of the fraction of rigid cells, f_r. From the slope of the curve in the main plot, we estimate the exponent $\beta \approx 0.194 \pm 0.007$, which is consistent with that for 2D random percolation, $\beta = 5/36$. The results were obtained for $N = 16384$ and averaged over 10 samples.

works [44,52]. We observe from the inset of Fig. 4 that the corresponding χ has a peak around $f_r^* \approx 0.534$, signaling the onset of percolation, in line with the results from the data collapse in Fig. 3. From a finite-size scaling analysis, using the shift of the peak in the variance (χ) with N, we estimate the threshold $f_r^* \approx 0.5353 \pm 0.0003$. Using this value, we calculate the scaling exponent (shown in the main plot), $\beta \approx 0.194 \pm 0.007$. Larger simulations are needed to estimate the exponents with higher precision, which is beyond the scope of this work. Nonetheless, the obtained value of β is consistent with that for random percolation, $\beta = 5/36$ [64,65].

In Fig. 2, we plot in white the line corresponding to $f_r^* \approx 0.5353$, which sets the percolation threshold for the disordered substrate. The gray line corresponds to $f_r^* \approx 0.21$ taken from Ref. [52] as the onset of rigidity in the cell disordered system. This highlights the differences between the two types of disorder and how they change the mechanical properties of the tissue. In the cell disordered case, the heterogeneity increases the tensions, $\tau \sim p_i - p_{0,i}$, leading to a more rigid tissue. For the substrate disorder, larger tensions can be observed at higher values of the disorder (σ) but the average tension in the tissue decreases. Furthermore, the distribution of tensions becomes more symmetrical, which promotes the fluid-like state (see the Supplemental Material [58]).

V. AVERAGED SUBSTRATE

In a cell tissue, one expects that one cell senses a region of the substrate rather than a single point. In order to account for this effect, we consider next the averaged substrate described in the methods section. The averaging is aimed to mimic the process through which a cell senses a given area under it and thus responds. To each square tile j in the averaged substrate corresponds a value of the shape index, $p_{0,j}$, which is the average of the shape index in the square tiles within a distance $\xi/2$ from j. The length scale ξ sets the diameter of the circle
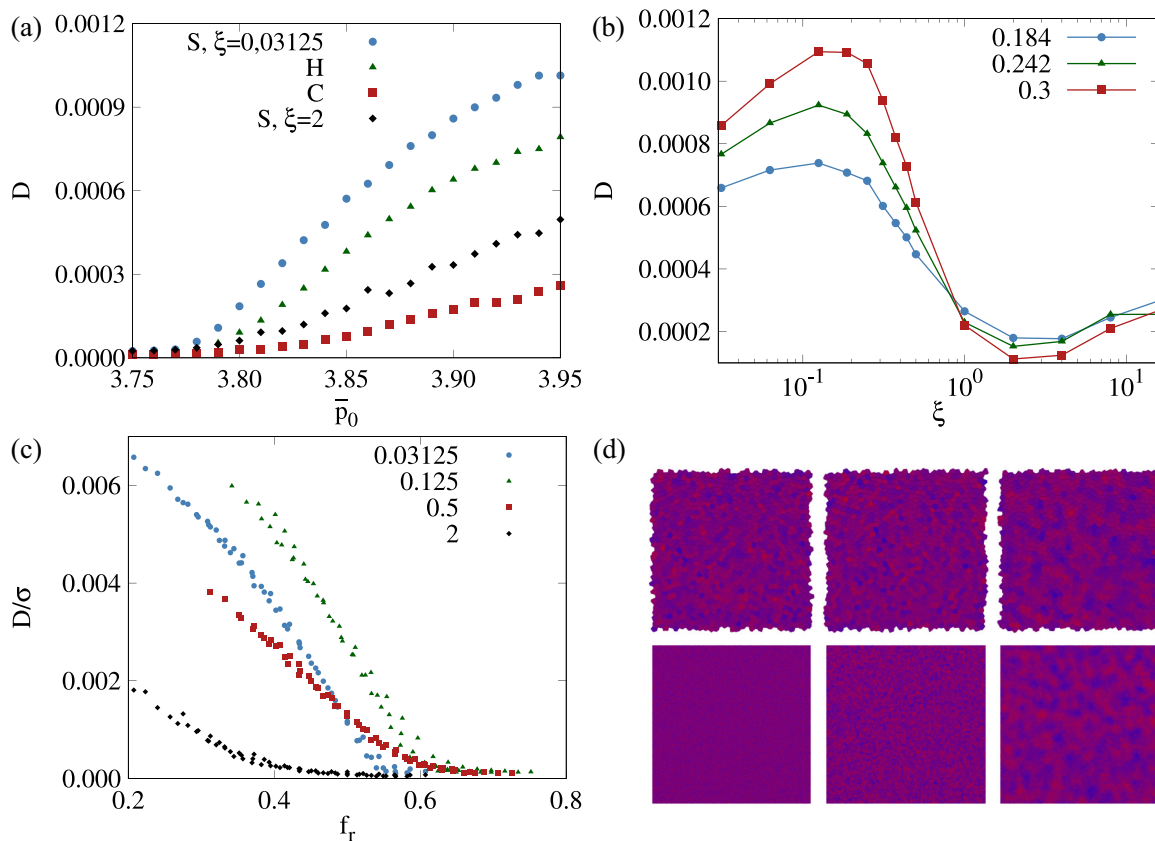
FIG. 5. Effect of substrate heterogeneities on cell motility. In panel (a) the diffusion coefficients are plotted for different types of heterogeneity: "S" is for substrate disorder, not averaged for a correlation length $\xi = 0.03125$ and averaged for $\xi = 2$. "C" is for cell disorder, as in Ref. [52], where each cell has a random shape index $p_{0,i}$ from a normal distribution, which remains constant. "H" is for the homogeneous tissue. Panel (b) illustrates how the diffusion coefficient varies with the substrate correlation length ξ, for a mean $\bar{p}_0 = 3.85$. In panel (c), the diffusion coefficient rescaled by the standard deviation (σ) is plotted as a function of the fraction of rigid cells, f_r, for four different correlation lengths, ξ. In panel (d) are schematic representations of the tissue (top) and the substrate (bottom) for correlation lengths $\xi = 0.125, 0.5, 2$ respectively. These results were obtained using $N = 1024$ and averaged over 10 different samples. We found that although the mechanical properties of the tissue change with the correlation length, ξ, the curves collapse with the fraction of rigid cells, f_r, suggesting that the percolation of rigid cells still drives the tissue rigidity. A correlation length of $\xi = 1$ is found above which the response of the tissue to the substrate disorder changes, with higher disorder, σ, leading to a more rigid tissue.

used to calculate the averaged substrate disorder and thus sets the correlation length (as discussed in the Supplemental Material [58]). Figure 5(d) shows some examples of averaged substrates (bottom row) with the corresponding tissues (top row).

Figure 5(a) depicts the diffusion coefficients measured for four different systems as a function of the mean, $\bar{p}_0$. We consider a random substrate (S, $\xi = 0.03125$), a homogeneous tissue (H), a tissue with cell disorder (C), and an averaged substrate (S, $\xi = 2$). Both substrate and cell disordered systems have a disorder dispersion $\sigma = 0.184$. We confirm that the cell disorder decreases the motility of the cells while the random substrate increases it. However, if the correlation length of the substrate is of the order of the typical cell diameter (or larger), then the cells become less mobile than in the homogeneous case. Thus, substrate disorder with large correlation lengths can also lead to more rigid tissues. In Fig. 5(b), this is shown for three different values of the standard deviation (σ). We find that while for correlation lengths lower than the typical cell diameter, $\xi < 1$, more disordered substrates lead to larger diffusion coefficients than in the homogeneous case,

for correlation lengths above the typical cell diameter, $\xi > 1$, substrate disorder decreases cell diffusion. This happens since for large correlation lengths the cells adapt to the substrate smoothly as the gradient of the shape index, $p_{0,i}$, is small. By contrast, for smaller correlation lengths, ξ, the cells change their shape index $p_{0,i}$ quite rapidly (the dependence of the diffusion coefficient with ξ is further explored in the Supplemental Material [58]). This leads to different behaviors of the tension distribution in the tissue. For $\xi < 1$, as the dispersion, σ, increases, the variance of the tensions also increases while its average value decreases promoting fluid-like tissues. For $\xi > 1$ the variance of the tensions is almost constant while their average value increases leading to more rigid tissues (see the Supplemental Material [58]).

Both types of behavior, however, are related to the percolation argument developed above. In Fig. 5(c), we report data for different values of the correlation length (ξ) which is collapsed using the same scaling as in Fig. 3. Thus, the behavior is driven by the percolation of rigid cells. As the correlation length (ξ) changes, the threshold values for the percolation transition also change [$\bar{p}_0^*(\xi)$ and $f_r^*(\xi)$]. We note

that for $\xi = 2$, where the tissue is the most rigid, the percolation threshold for the fraction of rigid cells, $f_r^* \approx 0.38$, tends to the value reported in Ref. [52], which is consistent with a more rigid tissue than for the homogeneous substrate.

VI. CONCLUSION

We studied the effects of spatial disorder of the cell-substrate interaction on the motility of the cells in a confluent tissue. We considered the self-propelled Voronoi model to describe the dynamics of cells in a confluent tissue. We hypothesize that the impact of a heterogeneous substrate can be described by a space-dependent shape index, where the preferred geometry of each cell, $p_{0,i}$, depends on its position. To model the spatial heterogeneities, we divided the surface of the substrate into square tiles, where each tile has a value of the shape index, $p_{0,j}$, drawn from a Gaussian distribution with mean $\bar{p}_0$ and standard deviation σ. We also considered a more realistic description of an averaged substrate, where cells respond to a local averaged disorder. We show that the larger the area probed by the cell, the smaller the effect of heterogeneity. This is in contrast to what is known for tissues with disorder in the mechanical properties of the cells. For those tissues, the rigidity increases with the level of disorder [52]. Our results suggest that, for smaller correlation lengths, the random change in the shape index leads to a more symmetrical tension distribution with lower average values, characteristic of more motile cells. For larger correlation lengths, the cells will have more time to adapt and the distribution of tensions shifts toward larger values characteristic of a more rigid tissue. We also note that for the largest values of the correlation length where the tissue is most solid-like, our results approach those of the cell disorder reported in Ref. [52]. This suggests that these two types of disorder are closely related.

We also show that our results for a given correlation length may be collapsed onto a single curve if we use the fraction of rigid cells [Eq. (5)] as the control parameter. This suggests that the changes to the mechanics of the tissue are a consequence of the percolation of rigid cells, characterized by a perimeter smaller than a given threshold $p_i < \bar{p}_0^*$. Using the fraction of rigid cells in the largest cluster, we obtained the threshold for the reported increase in motility, $f_r^* \approx 0.5353 \pm 0.0003$, for a completely random substrate without averaging, and a scaling exponent $\beta \approx 0.194 \pm 0.007$. For larger values of the correlation length, our results suggest that the value of the threshold changes. Due to the symmetries of the model and the short-range nature of the correlations in the spatial distribution of the disorder, we hypothesize that the percolation transition belongs to the 2D random percolation universality class as corroborated by the value of the obtained exponents.

Although we focused on changes to the shape index of the cells, p_0, it is expected that the substrate can affect other variables of the model (for example, v_0, μ, D_r, or A_0). We restrict our study to this parameter since there is clear experimental evidence suggesting that changes to cell shape impact on the cell motion and collective dynamics [16]. Furthermore, exploring all the possible parameters would render the model intractable. Previous works have also shown that the dynam-

ics of mixtures is much less sensitive to differences in cell area than perimeter [66]. Thus, we expect that changes to certain parameters will lead to more subtle and potentially less marked effects.

These results can play an important role not only in tissue engineering, where the mechanical properties of the tissue are important [2], but also in the study of cancer where cells change the surrounding ECM in order to enhance their motility. Our results suggest that the underlying structure supporting the tissue, either the ECM or a culture substrate, should not be described using generalized bulk metrics since heterogenieties can play a relevant role in the tissue mechanics. Although we used a simplistic approach, these results should be robust to different substrate geometries. This also extends to curved substrates as long as the curvature does not play a major role in the tissue rigidity, as reported in previous studies [67].

Recently, it was shown that the cell adaptation time sets a minimum scale for the differences on the substrate that a cell can probe [60]. Experimental values for the characteristic length of the changes in the substrate were used. Our results allow us to refine those calculations. The cell size sets the relevant length scale for adaptation, thus the typical size of epithelial cells in confluent tissues ($L \approx 20 \ \mu$m) sets the minimum length scale of the pattern for cells to be able to adapt. We can then calculate the expected adaptation time using the theory developed in Ref. [60]. Using a typical diffusion coefficient for tissue cells of the order of $D \approx 0.1 \ \mu\text{m}^2 \ \text{min}^{-1}$, we estimate that the typical time for a cell to adapt in a tissue interacting with a heterogeneous substrate is of the order of $\tau \approx 16$ h. We have no knowledge of such measurements for cells in confluent tissues, but they fall within the relevant ranges for single cells adapting to heterogeneous substrates [61].

Here, we focused on a 2D description, but a 3D generalization is possible. In a simple generalization of the model to 3D [68], we expect similar results since a fluid to solid transition is present and the cells are able to diffuse throughout the tissue. If we consider a more realistic description of a 3D epithelial monolayer, then we would need a vertex model along the lines of Ref. [69] and characterize the apical and basal sides of the cells differently. Then, it is expected that the competition between the basal and apical perimeter difference plays a role in the diffusion of the cells. This would be interesting to explore in future studies.

We have also neglected both cell death and division. Due to modeling constraints, it is required that the number of cells remains constant throughout the simulation. Other works explored the effect of cellular division [70], and in the context of disordered media, it would be interesting to focus on how cell division or death play a role in tissue cell motility.

[1] R. Langer and J. Vacanti, Tissue engineering, Science **260**, 920 (1993).

[2] C. F. Guimarães, L. Gasperini, A. P. Marques, and R. L. Reis, The stiffness of living tissues and its implications for tissue engineering, Nat. Rev. Mater. **5**, 351 (2020).

[3] T. Iskratsch, H. Wolfenson, and M. P. Sheetz, Appreciating force and shape—the rise of mechanotransduction in cell biology, Nat. Rev. Mol. Cell Biol. **15**, 825 (2014).

[4] E. Garreta, P. Prado, C. Tarantino, R. Oria, L. Fanlo, E. Martí, D. Zalvidea, X. Trepat, P. Roca-Cusachs, A. Gavaldà-Navarro, L. Cozzuto, J. M. Campistol, J. C. Izpisúa Belmonte, C. Hurtado del Pozo, and N. Montserrat, Fine tuning the extracellular environment accelerates the derivation of kidney organoids from human pluripotent stem cells, Nat. Mater. **18**, 397 (2019).

[5] C.-M. Lo, H.-B. Wang, M. Dembo, and Y.-L. Wang, Cell movement is guided by the rigidity of the substrate, Biophys. J. **79**, 144 (2000).

[6] D. E. Discher, P. Janmey, and Y. Wang, Tissue cells feel and respond to the stiffness of their substrate, Science **310**, 1139 (2005).

[7] W. Guo, M. T. Frey, N. A. Burnham, and Y. Wang, Substrate rigidity regulates the formation and maintenance of tissues, Biophys. J. **90**, 2213 (2006).

[8] S. Neuss, I. Blomenkamp, R. Stainforth, D. Boltersdorf, M. Jansen, N. Butz, A. Perez-Bouza, and R. Knüchel, The use of a shape-memory poly(ϵ-caprolactone)dimethacrylate network as a tissue engineering scaffold, Biomaterials **30**, 1697 (2009).

[9] D. T. Tambe, C. C. Hardin, T. E. Angelini, K. Rajendran, C. Y. Park, X. Serra-Picamal, E. H. Zhou, M. H. Zaman, J. P. Butler, D. A. Weitz, J. J. Fredberg, and X. Trepat, Collective cell guidance by cooperative intercellular forces, Nat. Mater. **10**, 469 (2011).

[10] M. Murrell, R. Kamm, and P. Matsudaira, Substrate viscosity enhances correlation in epithelial sheet movement, Biophys. J. **101**, 297 (2011).

[11] W. Song and J. F. Mano, Interactions between cells or proteins and surfaces exhibiting extreme wettabilities, Soft Matter **9**, 2985 (2013).

[12] R. Sunyer, V. Conte, J. Escribano, A. Elosegui-Artola, A. Labernadie, L. Valon, D. Navajas, J. M. García-Aznar, J. J. Muñoz, P. Roca-Cusachs, and X. Trepat, Collective cell durotaxis emerges from long-range intercellular force transmission, Science **353**, 1157 (2016).

[13] P. A. Janmey, D. A. Fletcher, and C. A. Reinhart-King, Stiffness sensing by cells, Physiol. Rev. **100**, 695 (2020).

[14] T. Yeung, P. C. Georges, L. A. Flanagan, B. Marg, M. Ortiz, M. Funaki, N. Zahir, W. Ming, V. Weaver, and P. A. Janmey, Effects of substrate stiffness on cell morphology, cytoskeletal structure, and adhesion, Cell Motil. Cytoskeleton **60**, 24 (2005).

[15] M. Guo, A. F. Pegoraro, A. Mao, E. H. Zhou, P. R. Arany, Y. Han, D. T. Burnette, M. H. Jensen, K. E. Kasza, J. R. Moore, F. C. Mackintosh, J. J. Fredberg, D. J. Mooney, J. Lippincott-Schwartz, and D. A. Weitz, Cell volume change through water efflux impacts cell stiffness and stem cell fate, Proc. Natl. Acad. Sci. U.S.A. **114**, E8618 (2017).

[16] J. Devany, D. M. Sussman, T. Yamamoto, M. L. Manning, and M. L. Gardel, Cell cycle–dependent active stress drives epithe-

lia remodeling, Proc. Natl. Acad. Sci. U.S.A. **118**, e1917853118 (2021).

[17] B. L. Doss, M. Pan, M. Gupta, G. Grenci, R.-M. Mège, C. T. Lim, M. P. Sheetz, R. Voituriez, and B. Ladoux, Cell response to substrate rigidity is regulated by active and passive cytoskeletal stress, Proc. Natl. Acad. Sci. U.S.A. **117**, 12817 (2020).

[18] K. A. Davis, K. A. Burke, P. T. Mather, and J. H. Henderson, Dynamic cell behavior on shape memory polymer substrates, Biomaterials **32**, 2285 (2011).

[19] L.-F. Tseng, P. T. Mather, and J. H. Henderson, Shape-memory-actuated change in scaffold fiber alignment directs stem cell morphology, Acta Biomaterialia **9**, 8790 (2013).

[20] H. Jeon, S. Koo, W. M. Reese, P. Loskill, C. P. Grigoropoulos, and K. E. Healy, Directing cell migration and organization via nanocrater-patterned cell-repellent interfaces, Nat. Mater. **14**, 918 (2015).

[21] P. Y. Mengsteab, K. Uto, A. S. T. Smith, S. Frankel, E. Fisher, Z. Nawas, J. Macadangdang, M. Ebara, and D.-H. Kim, Spatiotemporal control of cardiac anisotropy using dynamic nanotopographic cues, Biomaterials **86**, 1 (2016).

[22] S. H. Kim, J. Turnbull, and S. Guimond, Extracellular matrix and cell signalling: The dynamic cooperation of integrin, proteoglycan, and growth factor receptor, J. Endocrinol. **209**, 139 (2011).

[23] C. J. Miller and L. A. Davidson, The interplay between cell signalling and mechanics in developmental processes, Nat. Rev. Genet. **14**, 733 (2013).

[24] W. J. Hadden, J. L. Young, A. W. Holle, M. L. McFetridge, D. Y. Kim, P. Wijesinghe, H. Taylor-Weiner, J. H. Wen, A. R. Lee, K. Bieback, B.-N. Vo, D. D. Sampson, B. F. Kennedy, J. P. Spatz, A. J. Engler, and Y. S. Choi, Stem cell migration and mechanotransduction on linear stiffness gradient hydrogels, Proc. Natl. Acad. Sci. U.S.A. **114**, 5647 (2017).

[25] K. Wolf, M. te Lindert, M. Krause, S. Alexander, J. te Riet, A. L. Willis, R. M. Hoffman, C. G. Figdor, S. J. Weiss, and P. Friedl, Physical limits of cell migration: Control by ECM space and nuclear deformation and tuning by proteolysis and traction force, J. Cell Biol. **201**, 1069 (2013).

[26] S. Aznavoorian, M. L. Stracke, H. Krutzsch, E. Schiffmann, and L. A. Liotta, Signal transduction for chemotaxis and haptotaxis by matrix molecules in tumor cells, J. Cell Biol. **110**, 1427 (1990).

[27] J. T. Smith, J. T. Elkin, and W. M. Reichert, Directed cell migration on fibronectin gradients: Effect of gradient slope, Exp. Cell Res. **312**, 2424 (2006).

[28] P. P. Provenzano, D. R. Inman, K. W. Eliceiri, S. M. Trier, and P. J. Keely, Contact guidance mediated three-dimensional cell migration is regulated by Rho/ROCK-dependent matrix reorganization, Biophys. J. **95**, 5374 (2008).

[29] C. M. Kraning-Rush, J. P. Califano, and C. A. Reinhart-King, Cellular traction stresses increase with increasing metastatic potential, PLoS ONE **7**, e32572 (2012).

[30] K. R. Levental, H. Yu, L. Kass, J. N. Lakins, M. Egeblad, J. T. Erler, S. F. Fong, K. Csiszar, A. Giaccia, W. Weninger, M. Yamauchi, D. L. Gasser, and V. M. Weaver, Matrix crosslinking forces tumor progression by enhancing integrin signaling, Cell **139**, 891 (2009).

[31] P. Carmeliet and R. K. Jain, Angiogenesis in cancer and other diseases, Nature (London) **407**, 249 (2000).

[32] M. Egeblad and Z. Werb, New functions for the matrix metalloproteinases in cancer progression, Nat. Rev. Cancer **2**, 161 (2002).

[33] K. Wolf and P. Friedl, Mapping proteolytic cancer cell-extracellular matrix interfaces, Clin. Exp. Metastasis **26**, 289 (2009).

[34] C. M. Kraning-Rush, S. P. Carey, M. C. Lampi, and C. A. Reinhart-King, Microfabricated collagen tracks facilitate single cell metastatic invasion in 3D, Integr. Biol. **5**, 606 (2013).

[35] A. G. Fletcher, M. Osterfield, R. E. Baker, and S. Y. Shvartsman, Vertex models of epithelial morphogenesis, Biophys. J. **106**, 2291 (2014).

[36] R. Farhadifar, J.-C. Röper, B. Aigouy, S. Eaton, and F. Jü, The influence of cell mechanics, cell-cell interactions, and proliferation on epithelial packing, Curr. Biol. **17**, 2095 (2007).

[37] R. Alert and X. Trepat, Physical models of collective cell migration, Annu. Rev. Condens. Matter Phys. **11**, 77 (2020).

[38] B. A. Camley and W.-J. Rappel, Physical models of collective cell motility: From cell to tissue, J. Phys. D: Appl. Phys. **50**, 113002 (2017).

[39] D. Bi, J. H. Lopez, J. M. Schwarz, and M. L. Manning, Energy barriers and cell migration in densely packed tissues, Soft Matter **10**, 1885 (2014).

[40] D. Bi, J. H. Lopez, J. M. Schwarz, and M. L. Manning, A density-independent rigidity transition in biological tissues, Nat. Phys. **11**, 1074 (2015).

[41] A. J. Kabla, Collective cell migration: Leadership, invasion and segregation, J. R. Soc. Interface **9**, 3268 (2012).

[42] A. Hernandez, M. F. Staddon, M. J. Bowick, M. C. Marchetti, and M. Moshe, Geometric rigidity and anomalous elasticity of cellular tissue vertex model, arXiv:2109.10407 [cond-mat.soft].

[43] J. Huang, J. O. Cochran, S. M. Fielding, M. C. Marchetti, and D. Bi, Shear-Driven Solidification and Nonlinear Elasticity in Epithelial Tissues, Phys. Rev. Lett. **128**, 178001 (2022).

[44] D. Bi, X. Yang, M. C. Marchetti, and M. L. Manning, Motility-Driven Glass and Jamming Transitions in Biological Tissues, Phys. Rev. X **6**, 021011 (2016).

[45] D. M. Sussman, J. M. Schwarz, M. C. Marchetti, and M. L. Manning, Soft yet Sharp Interfaces in a Vertex Model of Confluent Tissue, Phys. Rev. Lett. **120**, 058001 (2018).

[46] S. Kaliman, C. Jayachandran, F. Rehfeldt, and A.-S. Smith, Limits of applicability of the Voronoi tessellation determined by centers of cell nuclei to epithelium morphology, Front. Psychol. **7**, 551 (2016).

[47] D. M. Sussman, M. Paoluzzi, M. C. Marchetti, M. L. Manning, M. C. Marchetti, and M. L. Manning, Anomalous glassy dynamics in simple models of dense biological tissue, Europhys. Lett. **121**, 36001 (2018).

[48] J.-A. Park, J. H. Kim, D. Bi, J. A. Mitchel, N. T. Qazvini, K. Tantisira, C. Y. Park, M. McGill, S.-H. Kim, B. Gweon, J. Notbohm, R. S. Jr, S. Burger, S. H. Randell, A. T. Kho, D. T. Tambe, C. Hardin, S. A. Shore, E. Israel, D. A. Weitz, D. J. Tschumperlin, E. P. Henske, S. T. Weiss, M. L. Manning, J. P. Butler, J. M. Drazen, and J. J. Fredberg, Unjamming and cell shape in the asthmatic airway epithelium, Nat. Mater. **14**, 1040 (2015).

[49] S. Grosser, J. Lippoldt, L. Oswald, M. Merkel, D. M. Sussman, F. Renner, P. Gottheil, E. W. Morawetz, T. Fuhs, X. Xie, S. Pawlizak, A. W. Fritsch, B. Wolf, L.-C. Horn, S. Briest, B. Aktas, M. L. Manning, and J. A. Käs, Cell and Nucleus Shape as an Indicator of Tissue Fluidity in Carcinoma, Phys. Rev. X **11**, 011033 (2021).

[50] D. T. Butcher, T. Alliston, and V. M. Weaver, A tense situation: Forcing tumour progression, Nat. Rev. Cancer **9**, 108 (2009).

[51] R. Sinkus, J. Lorenzen, D. Schrader, M. Lorenzen, M. Dargatz, and D. Holz, High-resolution tensor MR elastography for breast tumour detection, Phys. Med. Biol. **45**, 1649 (2000).

[52] X. Li, A. Das, and D. Bi, Mechanical Heterogeneity in Tissues Promotes Rigidity and Controls Cellular Invasion, Phys. Rev. Lett. **123**, 058101 (2019).

[53] G. Ciasca, T. E. Sassun, E. Minelli, M. Antonelli, M. Papi, A. Santoro, F. Giangaspero, R. Delfini, and M. De Spirito, Nanomechanical signature of brain tumours, Nanoscale **8**, 19629 (2016).

[54] C. Alibert, B. Goud, and J. B. Manneville, Are cancer cells really softer than normal cells?, Biol. Cell **109**, 167 (2017).

[55] E. W. Morawetz, R. Stange, T. R. Kießling, J. Schnauß, and J. A. Käs, Optical stretching in continuous flows, Converg. Sci. Phys. Oncol. **3**, 024004 (2017).

[56] S. M. Zehnder, M. Suaris, M. M. Bellaire, and T. E. Angelini, Cell volume fluctuations in MDCK monolayers, Biophys. J. **108**, 247 (2015).

[57] M. L. Manning, R. A. Foty, M. S. Steinberg, and E.-M. Schoetz, Coaction of intercellular adhesion and cortical tension specifies tissue surface tension, Proc. Natl. Acad. Sci. USA **107**, 12517 (2010).

[58] See Supplemental Material at http://link.aps.org/supplemental/10.1103/PhysRevResearch.4.023186 for the following additional information (1) Additional details regarding the simulations; (2) Statistichal properties of the random substrate; (3) Additional information regarding the contact percolation of cells and tension distribution; and (4) Additional results for the cell disorder case in the Voronoi model.

[59] M. Merkel, K. Baumgarten, B. P. Tighe, and M. L. Manning, A minimal-length approach unifies rigidity in underconstrained materials, Proc. Natl. Acad. Sci. U.S.A. **116**, 6560 (2019).

[60] D. E. Pinto, G. Erdemci-Tandogan, M. L. Manning, and N. A. Araújo, The cell adaptation time sets a minimum length scale for patterned substrates, Biophys. J. **119**, 2299 (2020).

[61] M. Ebara, Shape-memory surfaces for cell mechanobiology, Sci. Technol. Adv. Mater. **16**, 014804 (2015).

[62] D. M. Sussman, CELLGPU: Massively parallel simulations of dynamic vertex models, Comput. Phys. Commun. **219**, 400 (2017).

[63] D. M. Sussman and M. Merkel, No unjamming transition in a Voronoi model of biological tissue, Soft Matter **14**, 3397 (2018).

[64] D. Stauffer and A. Aharony, *Introduction to Percolation Theory* (Taylor and Francis, Philadelphia, 2018).

[65] M. Sahini and M. Sahimi, *Applications of Percolation Theory* (CRC Press, Boca Raton, FL, 1994).

[66] P. Sahu, D. M. Sussman, M. Rübsam, A. F. Mertz, V. Horsley, E. R. Dufresne, C. M. Niessen, M. C. Marchetti, M. L. Manning, and J. M. Schwarz, Small-scale demixing in confluent biological tissues, Soft Matter **16**, 3325 (2020).

[67] D. M. Sussman, Interplay of curvature and rigidity in shape-based models of confluent tissue, Phys. Rev. Research **2**, 023417 (2020).

[68] M. Merkel and M. L. Manning, A geometrically controlled rigidity transition in a model for confluent 3D tissues, New J. Phys. **20**, 022002 (2018).

[69] S. Okuda and K. Fujimoto, A mechanical instability in planar epithelial monolayers leads to cell extrusion, Biophys. J. **118**, 2549 (2020).

[70] M. Czajkowski, D. M. Sussman, M. C. Marchetti, and M. L. Manning, Glassy dynamics in models of confluent tissue with mitosis and apoptosis, Soft Matter **15**, 9133 (2019).